Spectroscopic properties of Mg 3*pns* autoionizing states

C. J. Dai
Department of Physics, Zhejiang University, Hangzhou 310027, People's Republic of China
(Received 27 September 1994)

We present a study of characteristics of autoionization spectra for the Mg 3*pns* Rydberg series. The calculations were performed using multichannel quantum-defect theory combined with two versions of K matrices. The systematic investigation of states from the lower- to higher-lying members of the Mg 3*pns* Rydberg series allows one to reach a deeper understanding of physical manifestations involved. The calculations permit a detailed interpretation of recent experimental measurements in atomic magnesium. Energy levels are identified and assigned to the Mg 3*pns* autoionizing states for n greater than 6. A comparison with available experiments is provided.

PACS number(s): 32.80.Dz, 32.80.Fb, 31.20.Di

I. INTRODUCTION

For the past two decades, the autoionization process of the alkaline-earth elements has drawn much attention of physists [1–5]. However, due to experimental inconvenience, only recently the total and differential cross sections of autoionization for the lighter elements, such as atomic Mg, have been studied intensively [6–9], which makes a comparison between the experiment and theory possible.

The line shapes of the transitions from the Mg 3*sns* to the 3*pns* autoionizing Rydberg states were studied experimentally and reached excellent agreement with multichannel quantum-defect theory (MQDT) [6]. However, the energy levels of the Mg $3p_j ns$ autoionizing states were not given there. To our knowledge, the Mg 3*pns* states were only identified for $n=4-12$ without the resolution of the $3p_j$ core fine structures [10], where $j=\frac{1}{2}$ or $\frac{3}{2}$. Furthermore, the study of the 3*pns* autoionizing states is especially appealing as $J=1$ is the only allowed final excited-state angular momentum. In this paper, we present a study of the energy levels of the 3*pns* autoionizing states with the $3p_j$ fine structures resolved. Taking advantage of recently published experimental data for the Mg 3*sns* $^1S_0$ Rydberg states [6], we have systematically investigated the spectra of the Mg 3*pns* autoionizing states for $n=6-22$. The assignments of energy levels to the $3p_j ns$ states are given with the full widths at half maximum (FWHM) of their profiles. In addition, the variations of quantum defects for each autoionizing Rydberg series and various manifestations due to configuration interactions (CI's) are demonstrated. The physical insight under these phenomena is explored and discussed.

MQDT was first introduced by Seaton [11,12] as an empirical approach. Since then it has been reformulated by Fano and co-workers [13–15]. In the early stages of its development, applications of MQDT involved the empirical determination of a set of parameters representing the interaction between specific channels by fitting the measured peak positions and widths of Rydberg states. MQDT treats the bound autoionizing states and the adjoining continuum states in a unified fashion and enjoys great success in various applications.

Over the past decade, MQDT, combined with the R matrix [16–19], has been used with extraordinary success in predicting the photoabsorption cross sections of alkaline-earth atoms in the energy range up to about 5 eV above the lowest ionization limit. Applications on various molecular systems [16,20] performed by Greene and co-workers were also quite successful. In this paper, we used precalculated K matrices [6,9] to derive the MQDT parameters $U_{i\alpha}$ and μ_α necessary for carrying out our study.

The combination of MQDT with the precalculated K matrices has been utilized to calculate the spectra of the Mg 3*pns* autoionizing states. The comparison between the theory and available experimental data for those states is made to seek the possibilities of improving the K matrices. The K matrix, as we know, was transformed from the R matrix calculated within a certain reaction volume V_0. The radius of V_0, called r_0, is critical to the R-matrix calculation, the K-matrix calculation, and the final results of MQDT treatments. The possible impacts of the r_0 value on the Mg 3*pns* spectra have been investigated using two versions of K matrices, with $r_0=12$ and 20 a.u., respectively.

II. THEORETICAL FRAMEWORK

Nowadays, calculations of autoionization spectra for the alkaline-earth atoms may follow a standard routine of MQDT, whose parameters may be determined by transforming the K matrix. Here we do not intend to give a complete description of the theory. Instead we only briefly outline the relevant portions of the theory for the sake of convenience to discuss results in Sec. III. The readers interested are directed to Refs. [16–19] for a full exposition of the theory.

The K matrix taken from either Ref. [6] or [9] is for the three LS-coupled terms by which the $J=1$, odd-parity, $3s\varepsilon p$, 3*pns*, and 3*pnd* configurations may be described. The elements of the matrix are slowly varying functions of energy and are given at three energies, which cover a wide range of 4400 cm^{-1}. In our calculation, as stated in

Ref. [6], interpolation or extrapolation is necessary to obtain a K matrix at all the energies we need. The matrix is provided in the LS-coupled form; we transform it to the jj-coupled form most suitable for MQDT analysis of autoionization spectra.

Diagonalization of a K matrix in the jj coupling gives directly two sets of MQDT parameters $U_{i\alpha}$ and μ_α. Interpretations of these parameters as a function of energy give rise to valuable insight into the underlying dynamics of the system, as well as providing energy levels, oscillator strengths, etc. $U_{i\alpha}$, an element of the unitary transformation matrix U, connects the ith collision channel and the αth eigenchannel. μ_α is the quantum defect of the α channel. The two sets of parameters are related by

$$\det\{U_{i\alpha}\sin[\pi(\nu_i+\mu_\alpha)]\}=0 \ . \tag{1}$$

For a closed channel, ν_i is the effective quantum number of the ith channel; for an open channel, $\nu_i=-\tau_\rho$, where $\pi\tau_\rho$ is the phase shift for the ρth open channel.

The wave function of a final state is described by the mixing coefficients $A_i^{(\rho)}$ or $B_\alpha^{(\rho)}$. $[A_i^{(\rho)}]^2$, usually called the spectral density, plays an important role in final autoionization spectra, which may be determined by

$$A_i^{(\rho)}=\sum_\alpha U_{i\alpha}\cos[\pi(\nu_i+\mu_a)]B_a^{(\rho)} \ , \tag{2}$$

where ρ runs from 1 to 2 since we have two open channels; ν_i is related to the bound energy W_i with

$$W_i=-R/\nu_i^2 \ , \tag{3}$$

where R is the mass-corrected Rydberg constant for atomic Mg. The simultaneous solutions of Eqs. (1) and (3) immediately yield the energy positions of every autoionizing state.

In this paper, a seven-channel MQDT model is used to study the Mg $3pns$, $J=1$ states. The assignments of seven channels are given in Table I.

In the case of energy below the Mg $3p_{1/2}$ ionization limit, the first two jj-coupled channels in Table I are open and the rest of the channels are closed. In this energy region, the principal quantum number n of the Mg $3p_{1/2}nl$ Rydberg series may be up to 35, which infers that the interactions between the two series converging to the $3p_{1/2}$ and $3p_{3/2}$ limits cover a great number of Rydberg states.

With the above knowledge, one may obtain the dipole matrix elements D_i and then the cross section of photoionization. D_i is the product of radial and angular parts of the dipole matrix element. In our case, the radial parts for two core transitions $3s_{1/2}\rightarrow 3p_j$ are virtually the same, which yields a constant contribution to the final spectrum. On the other hand, the angular parts, called overlap integrals, may be expressed as

$$O_j=\frac{2(\nu\nu_j)^2\sin\pi(\nu_j-\nu)}{\nu^{3/2}\pi(\nu_j^2-\nu^2)} \ , \tag{4}$$

where $j=\frac{1}{2}$ or $\frac{3}{2}$. Physically, O_j represents the spatial overlap between the wave functions of the outer electron before and after the core excitation. ν_j are the effective quantum numbers relative to the $3p_{1/2}$ or $3p_{3/2}$ ion limits (at 35 669 and 35 761 cm^{-1}, respectively).

Finally one is able to obtain the cross section for excitation of the doubly excited state, i.e.,

$$\sigma\propto\omega\sum_{\rho=\{n_c\}}\left|\sum_{i=3,4}D_iA_i^{(\rho)}\right|^2 \ , \tag{5}$$

where ω is the laser frequency of the core excitation and n_c is the number of open channels. Variation of σ with energy gives rise to the autoionization spectra of the Mg $3pns$ states, from which the peak positions and widths may be determined with great confidence. It is found that the classification of all the peaks with their quantum defects relevant to the $3p_j$ limits may assist in assigning them to different $3p_jns$ states. It is useful especially for the higher-n states with $n>15$. For the lower-n states, the profiles of the features (including their shapes and widths) are found to be more helpful than quantum defects in determining which state a peak should be assigned to. The details of our assignments are described in the next section.

III. RESULTS AND DISCUSSION

One of the advantages of MQDT is to treat all the states in terms of channels, each channel containing an infinite number of states characterized by a nearly energy-independent quantum defect. Generally, a spectrum of an autoionizing state contains contributions from all the possible channels. One may in turn decompose a spectrum into several components in terms of channels. As a result, one may easily understand the physical processes under the shadow of complex manifestations. Figures 1 and 2 show two examples of such an attempt.

Figure 1 contains the spectrum of the $3p_j12s$ autoionizing state, with which spectra of two spectral densities A_3^2 and A_4^2, corresponding to the $3p_jns$ channels, are put together. In order to obtain a whole picture, the two overlap integral squareds $O_{1/2}^2$ and $O_{3/2}^2$ are placed at the top of the figure. Examination of Fig. 1 shows immediately that the features of σ can be classified into two groups: the left one is mainly from A_3^2 or the $3p_{1/2}12s$ state and the other one is overwhelmingly from A_4^2 or the $3p_{3/2}12s$ state.

TABLE I. Assignments of $J=1$ channels in LS and jj couplings.

Coupling \ Labeling	1	2	3	4	5	6	7
$\|i\rangle$	$3s_{1/2}\varepsilon p_{1/2}$	$3s_{1/2}\varepsilon p_{3/2}$	$3p_{1/2}ns_{1/2}$	$3p_{3/2}ns_{1/2}$	$3p_{1/2}nd_{3/2}$	$3p_{3/2}nd_{3/2}$	$3p_{3/2}nd_{5/2}$
$\|a\rangle$	$3s\varepsilon p\ ^1P_1$	$3pns\ ^1P_1$	$3pnd\ ^1P_1$	$3s\varepsilon p\ ^3P_1$	$3pns\ ^3P_1$	$3pnd\ ^3P_1$	$3pnd\ ^3D_1$

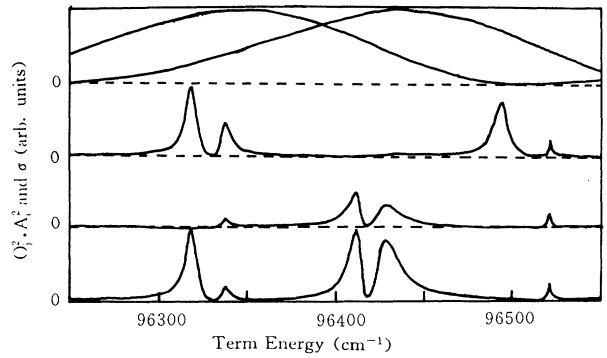

FIG. 1. Line shape of the $3s12s \rightarrow 3p_j12s$ transition. From the top to the bottom the spectra are for O_j^2, A_3^2, A_4^2, and σ_{3p12}, respectively, where $j=\frac{1}{2}$ and $\frac{3}{2}$.

On the other hand, the $3p_jns$ features are clearly located below their corresponding O_j^2 profiles, which independently indicate their own characters. Furthermore, the $3p_{1/2}13s$ feature does not appear in the final spectrum as expected since it locates near 96 500 cm^{-1}, where $O_{1/2}^2$ reduces to zero.

Precise assignments of spectral features may be much more apparent if one examines Fig. 2, which shows the spectra of the $3p_j12s$ autoionizing state and spectral densities of all bound channels. Obviously, two broad features may be identified as the $3p_{1/2}12s$ and $3p_{3/2}12s$ states, respectively. All the sharp features in the figure are due to configuration mixing with the Mg 3*pnd* $J=1$ states. This is evident if one examines the contributions from various channels.

Note that the widths of the 3*pns* and 3*pnd* states with the same n value are substantially different due to their distinct coupling strengths with the $3s\varepsilon p_j$ continuum channels. Stated more explicitly, these 3*pns* autoionizing states decay much faster than the 3*pnd* states to the $3s\varepsilon p_j$ continua. This phenomenon may be understood in a simple classical picture. Since the *ns* electron corresponds to the larger eccentricity of the elliptical orbit or smaller perihelion distance, the overlap between the 3*pns* and $3s\varepsilon p$ radial wave functions is significantly better than that between the 3*pnd* and $3s\varepsilon p$ radial wave functions, leading to the higher autoionization rate of the 3*pns* states and a broader spectral feature. Note that since the magnitudes of the 3*pnd* features are much greater than those of the 3*pns* features, to bring them together in the same scale requires one to artificially magnify the A_i^2 relevant to the 3*pns* channels. As a result, only the energy positions of A_i^2 in Fig. 2 are of interest to us.

To investigate the interactions between the Rydberg series converging to the $3p_j$ ionization limits as well as those between different channels in a quantitative manner, it is helpful to calculate how much contribution each channel makes to a specific $3p_jns$ spectral feature. Tables II and III are results of this kind; detailed descriptions of assignments of the levels tabulated will be furnished later. One may see from Tables II and III that almost none of the 3*pns* features contain solely a contribution from a single channel. Actually, the excitations of the 3*pnd* states are profound in many cases. This is due to the nonpure character of the initial state of the excitation. In some cases, different series make a comparable contribution to a final 3*pns* feature, which means that there exists heavy mixing between two $3p_jnl$ series. On the other hand, the $3p_jns$ and $3p_jnd$ channels converging to the same $3p_j$ limit sometimes share a single 3*pns* feature, which indicates strong coupling between channels. Above all, CIs are not only extensive, but also intensive for the Mg 3*pns* autoionizing Rydberg series. This sort of manifestation was observed previously in the case of the Mg 3*pnd* ($J=3$) series [7]. As explained in the 3*pnd* cases [7,8], a very small $3p_j$ fine-structure splitting (~ 92 cm^{-1}) is responsible for strong CIs in atomic magnesium. As a reference, atomic barium has a very

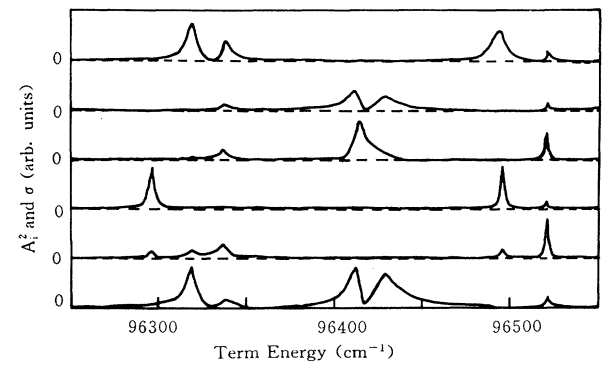

FIG. 2. Illustration of the classification of the features in terms of the calculated constituent spectral density. The spectral densities for the five bound channels are calculated as a function of term energy. From the top to the bottom the spectra are A_3^2 to A_7^2, and σ_{3p12s}, respectively. Some peaks in the final spectra originate from common features in several spectral densities.

TABLE II. Configuration mixing of five bound channels for the $3p_{1/2}ns$ series.

n	E (cm^{-1})	A_3^2	A_4^2	A_5^2	A_6^2	A_7^2
6	91 588.4	0.58	0.22	0.06	0.00	0.14
7	93 544.3	0.83	0.17	0.00	0.00	0.00
8	94 650.5	0.89	0.11	0.00	0.00	0.00
9	95 332.5	0.92	0.08	0.00	0.00	0.00
10	95 785.3	0.87	0.06	0.00	0.00	0.07
11	96 102.1	0.74	0.06	0.06	0.00	0.14
12	96 318.1	0.64	0.00	0.00	0.06	0.30
13	96 493.4	0.51	0.00	0.00	0.39	0.10
14	96 625.4	0.94	0.00	0.00	0.00	0.06
15	96 724.3	0.77	0.23	0.00	0.00	0.00
16	96 810.0	0.88	0.12	0.00	0.00	0.00
17	96 879.1	0.75	0.05	0.06	0.00	0.14
18	96 931.5	0.63	0.00	0.00	0.28	0.09
19	96 977.3	0.90	0.05	0.00	0.00	0.05
20	97 016.0	0.90	0.10	0.00	0.00	0.00
21	97 048.6	0.74	0.00	0.00	0.00	0.26
22	97 076.3	0.92	0.08	0.00	0.00	0.00

TABLE III. Configuration admixture of five bound channels for the $3p_{3/2}ns$ series.

n	E (cm^{-1})	A_3^2	A_4^2	A_5^2	A_6^2	A_7^2
6	91 872.6	0.20	0.69	0.05	0.00	0.06
7	93 708.5	0.12	0.78	0.05	0.00	0.05
8	94 780.6	0.08	0.83	0.04	0.00	0.05
9	95 443.6	0.05	0.87	0.04	0.00	0.04
10	95 885.4	0.00	0.90	0.10	0.00	0.00
11	96 193.4	0.00	0.85	0.15	0.00	0.00
12	96 428.9	0.00	0.61	0.28	0.00	0.11
13	96 592.7	0.05	0.84	0.05	0.00	0.06
14	96 720.7	0.31	0.69	0.00	0.00	0.00
15	96 822.8	0.06	0.86	0.00	0.00	0.08
16	96 902.9	0.00	0.64	0.34	0.00	0.00
17	96 971.1	0.13	0.81	0.00	0.00	0.06
18	97 025.2	0.00	0.95	0.05	0.00	0.00
19	97 071.0	0.08	0.86	0.00	0.00	0.06
20	97 108.1	0.00	0.89	0.11	0.00	0.00
21	97 141.7	0.15	0.76	0.00	0.00	0.09
22	97 168.8	0.22	0.78	0.00	0.00	0.00

large $6p_j$ fine-structure splitting ($\sim$1690 cm^{-1}) so that the $6p_{1/2}ns$ series solely interacts with the lowest members of the $6p_{3/2}ns$ ($n<10$) series. In contrast, the Mg $3p_{1/2}ns$ series interacts with all member of the $3p_{3/2}ns$ series, where n is up to 35.

To test the theory, we make a comparison with the experiment [6] and reach good agreement with it. In calculations we have employed two versions of K matrices with $r_0=12$ a.u. [6] and 20 a.u. [9], respectively, to observe the impacts by the choice of r_0. Figures 3 and 4 show two examples of the performance. They expose the properties of the $3p_j6s$ and $3p_j11s$ autoionizing states. In Fig. 4 the experimental spectrum is put in for handy comparison. Detailed examinations of many $3pns$ states ($n=6$–22) reveal that two versions of K matrices give virtually the same results for most of the states, as expected. However, the differences between the two-version calculations are profound for the lowest members of the $3pns$ states. For those states, the experimental

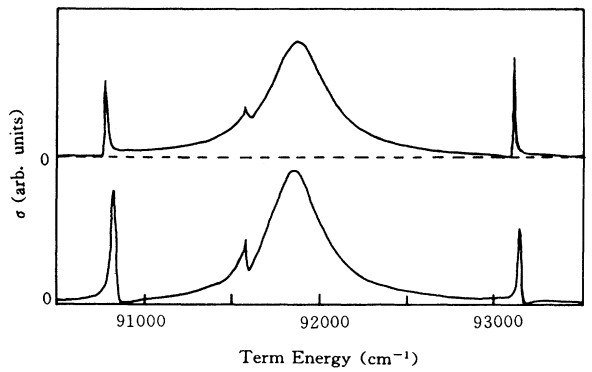

FIG. 3. Line shape of the $3s6s\rightarrow 3p_j6s$ transition. The top one is from the K matrix with $r_0=12$ a.u., the bottom is from the K matrix with $r_0=20$ a.u.

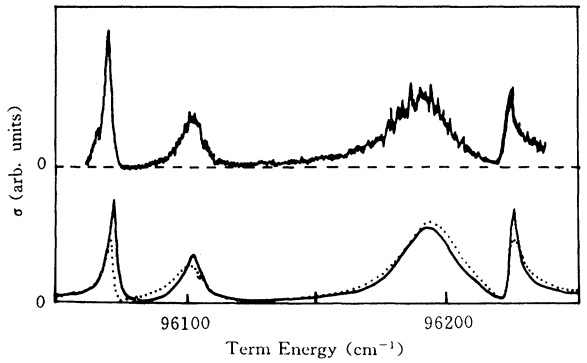

FIG. 4. Line shape of the $3s11s\rightarrow 3p_j11s$ transition. Two calculated spectra in the bottom are from the K matrices with $r_0=12$ a.u. (dashed line) and 20 a.u. (solid line), respectively. The experimental spectrum [6] is shown on the top for direct comparison.

spectra with resolution of the $3p_j$ fine structures have been unavailable, making a direct and systematic comparison difficult. To our knowledge, only a few calculations and experiments for the lowest members ($n=4$–5) of the $3pns$ and $3pnd$ ($J=1$) series by means of multiphoton ionization, are available [21–23]. It is apparent from Figs. 3 and 4 that the smaller r_0 is in better agreement with the experiments, which is understandable if one recalls the process of generating the R matrix and then the K matrix. The K matrix with small r_0 makes final spectra more accurate, whereas the K matrix with a large r_0, taking into account higher-order interactions neglected in the small-r_0 K matrix, is less accurate due to divergence of the wave functions as r increases. Thus, for the lower-n states, autoionizing states lying energetically lower, the profound dominance of short-range interactions is expected. The above manifestations indicate that $r_0=12$ a.u. is large enough to enclose all of the "correlated" regions in which the probability of finding two electrons is non-negligible.

Now we are in a position of assigning all the $3pns$ spectral features to correct $3p_jns$ states. We have performed configuration assignments with three different approaches. First, we calculated many spectra of the $3pns$ states, n ranging from 6 to 22, and merged them in a suitable way so that we could clearly see the patterns of the $3pns$ and $3pnd$ profiles. Starting from the lowest $3pns$ state in this study, where states with different quantum numbers are impossible to confuse, one may assign each peak with considerable confidence. Figures 5 and 6 show two examples of such performances, which cover most of the states concerned here. However, for the peaks lying energetically higher, the situation becomes more complicated. More explicitly, the spacings between successive Rydberg states are comparable with the ion fine-structure splitting; the widths of the $3p_jns$ states are comparable with those of the $3p_j(n-1)d$ autoionizing states. The regularity of spectral patterns becomes ambiguous, which is most evident for n around 14. In this n region the spectra indeed exhibit noticeable interference effects due to the overlap interference [6].

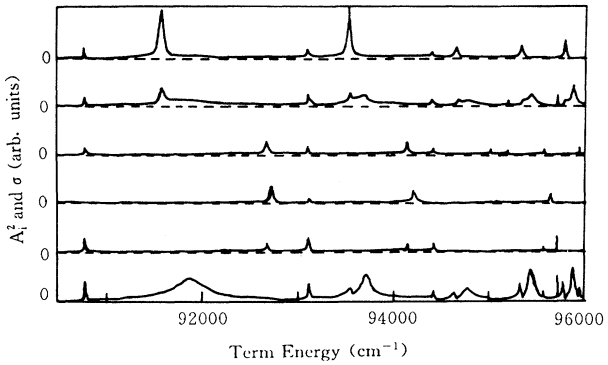

FIG. 5. Line shapes of the $3sns \rightarrow 3p_j ns$ transitions, where n is from 6 to 10. Spectral densities for the five bound channels are calculated to assist in identifying each peak. From the top to the bottom the spectra are for A_3^2 to A_7^2, and $\sigma_{3p_j ns}$, respectively. Again, some peaks in the final spectra originate from common features in several spectral densities.

Under these circumstances, a more reliable way is to sort peaks by their quantum defects, which are in general a constant for high-lying autoionizing states in any Rydberg series. An alternative approach to avoid possible confusion is to calculate the configuration admixture coefficients to find out the profound dominance of one or two channels, as shown in Tables II and III. Armed with these approaches, one is able to assign all the peaks to the 3*pns* or 3*pnd* autoionizing states confidently.

The results of the assignments are shown in Tables IV and V. There are corresponding to two versions of K matrices with $r_0 = 12$ and 20 a.u., respectively. In the tables the quantum defects (QDs) and the FWHM widths of states are also tabulated. For the purpose of comparison, in Table VI the experimental energy levels and widths extracted from the experiment of the line-shape study [24] are shown.

The energy levels predicted by the two versions of K matrices furnished a quantitative way for verification of some findings in Sec. II. Both versions reach satisfactory agreement with the experiment to some extent, either for energy levels or widths. We also noticed that there are small shifts in energy between resonance peaks of the theory and experiment for several autoionizing states.

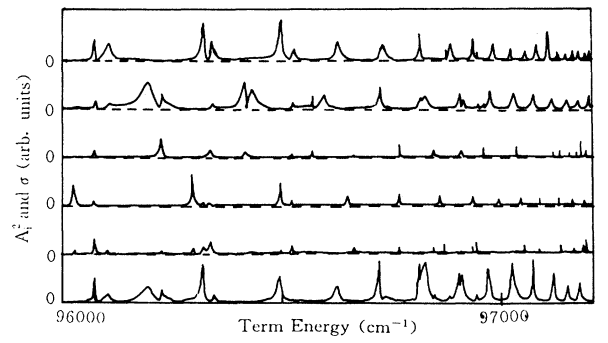

FIG. 6. Same as Fig. 5, except these spectra are the line shapes for the $3sns \rightarrow 3p_j ns$ transitions, where n is from 11 to 22.

TABLE IV. Energies and widths (FWHM) of Mg 3*pns* autoionizing states in cm^{-1} (calculated with a K-matrix of $r_0 = 12$ a.u.).

	Mg $3p_{1/2}ns$ states			Mg $3p_{1/2}ns$ states		
n	Energy	QD	Width	Energy	QD	Width
6	91 588.4	1.63	44.0	91 872.6	1.56	400.4
7	93 544.3	1.62	34.1	93 708.5	1.57	126.4
8	94 650.5	1.61	26.0	94 780.6	1.57	122.1
9	95 332.5	1.60	13.2	95 443.6	1.57	74.1
10	95 785.3	1.60	17.7	95 885.4	1.57	46.5
11	96 102.1	1.58	12.8	96 193.4	1.58	26.6
12	96 318.4	1.63	7.2	96 428.9	1.53	15.2
13	96 493.4	1.61	8.8	96 592.7	1.56	15.2
14	96 625.4	1.60	9.6	96 720.7	1.57	6.4
15	96 724.3	1.63	12.0	96 822.8	1.56	15.2
16	96 810.0	1.59	2.4	96 902.9	1.58	4.9
17	96 879.1	1.55	3.3	96 971.1	1.55	4.8
18	96 931.5	1.58	3.1	97 025.2	1.55	7.0
19	96 977.3	1.57	5.2	97 071.0	1.53	3.6
20	97 016.0	1.55	1.6	97 108.5	1.54	4.0
21	97 048.0	1.57	1.2	97 141.7	1.52	2.8
22	97 076.3	1.54	2.4	97 168.8	1.53	1.2

The widths given in tables follow a dependence on the quantum number n as qualitatively expected. For the $3pns\ ^1P_1$ series, the width of a state decreases with increasing number n, due to the weaker electron-electron Coulombic interaction, as a consequence of the decreasing overlap of their orbitals. In general, the calculated widths are found to be larger than those of the experiment. It is worth noting that in some regions the widths of the $3p_j ns$ states do not follow the mentioned tendency.

TABLE V. Energies and widths (FWHM) of Mg 3*pns* autoionizing states in cm^{-1} (calculated with a K-matrix of $r_0 = 20$ a.u.).

	Mg $3p_{1/2}ns$ states			Mg $3p_{1/2}ns$ states		
n	Energy	QD	Width	Energy	QD	Width
6	91 588.4	1.63	24.0	91 852.6	1.57	360.4
7	93 546.3	1.62	18.2	93 714.5	1.57	186.2
8	94 650.5	1.61	18.0	94 788.6	1.57	102.1
9	95 332.5	1.60	14.2	95 441.6	1.57	61.1
10	95 786.1	1.59	12.1	95 883.8	1.58	39.3
11	96 102.9	1.58	8.0	96 191.8	1.59	24.0
12	96 317.6	1.63	7.2	96 428.9	1.53	11.7
13	96 492.6	1.61	6.4	96 592.7	1.56	11.2
14	96 625.4	1.60	7.2	96 720.7	1.57	4.8
15	96 725.1	1.63	12.8	96 823.6	1.56	11.2
16	96 810.0	1.59	2.4	96 902.9	1.58	4.3
17	96 879.1	1.55	2.4	96 971.1	1.55	4.1
18	96 931.5	1.58	3.1	97 025.2	1.55	6.2
19	96 977.3	1.57	4.0	97 071.0	1.53	2.8
20	97 016.0	1.55	0.8	97 108.1	1.55	3.2
21	97 047.6	1.58	1.6	97 141.7	1.52	2.8
22	97 076.3	1.54	2.4	97 168.8	1.53	1.2

TABLE VI. Energies and widths (FWHM) of Mg $3pns$ autoionizing states from the experiment [24] (in cm^{-1}).

	Mg $3p_{1/2}ns$ states			Mg $3p_{3/2}ns$ states		
n	Energy	QD	Width	Energy	QD	Width
10	95 786.1	1.59	15.1	95 883.8	1.58	42.8
11	96 102.9	1.58	13.0	96 191.8	1.59	25.1
12	96 317.6	1.63	3.8	96 428.9	1.53	9.4
13	96 492.6	1.61	4.1	96 592.7	1.56	10.1
14	96 625.4	1.60	6.5	96 720.7	1.57	4.7
15	96 725.1	1.63	12.7	96 823.6	1.56	9.8
16	96 810.0	1.59	1.9	96 902.9	1.58	3.8
17	96 879.1	1.55	2.1	96 971.1	1.55	3.8
18	96 931.5	1.58	2.8	97 025.2	1.55	5.6

For instance, widths of the $3p_j14s$ and $3p_j15s$ states behave quite differently. The widths are changed dramatically around these states because of the "overlap interference" mentioned earlier. The manifestation may be explained by the fact that there is a coincidence that the spacing between the $n=14$ and 15 states matches the ion fine-structure splitting.

IV. CONCLUSION

We have presented a systematic study of the spectroscopic characteristics of the Mg $3pns$ autoionizing Rydberg states. The combination of MQDT with the K matrix enjoys great success in predicting energy levels and widths as well as providing a detailed interpretation of physical manifestations for the series. The calculations allow one to identify and designate all the spectral features with great reliability. The study also shows that the improvements for experiment and theory are desirable.

ACKNOWLEDGMENTS

This work was supported by the National Natural Science Foundation of China, the State Commission of Education of China, and The Science Foundation of Zhejiang University.

[1] R. R. Jones, C. J. Dai, and T. F. Gallagher, Phys. Rev. A **41**, 316 (1990).
[2] C. J. Dai, S. M. Jaffe, and T. F. Gallagher, J. Opt. Soc. Am. B **6**, 1486 (1989).
[3] E. Y. Xu, Y. Zhu, O. C. Mullins, and T. F. Gallagher, Phys. Rev. A **33**, 2401 (1986).
[4] Y. Zhu, E. Y. Xu, and T. F. Gallagher, Phys. Rev. A **36**, 3571 (1987).
[5] V. Lange, U. Eichmann, and W. Sandner, J. Phys. B **22**, 2245 (1989).
[6] G. W. Schinn, C. J. Dai, and T. F. Gallagher, Phys. Rev. A **43**, 2316 (1991).
[7] C. J. Dai, G. W. Schinn, and T. F. Gallagher, Phys. Rev. A **42**, 223 (1990).
[8] M. D. Lindsay *et al.*, Phys. Rev. A **45**, 231 (1992).
[9] M. D. Lindsay *et al.*, Phys. Rev. A **46**, 3789 (1992).
[10] V. Kaufman and W. C. Martin, J. Phys. Chem. Ref. Data **20**, 83 (1991).
[11] M. J. Seaton, Proc. Phys. Soc. London **88**, 801 (1966).
[12] M. J. Seaton, Rep. Prog. Phys. **46**, 167 (1983).
[13] U. Fano and C. M. Lee, Phys. Rev. Lett. **31**, 1573 (1973); U. Fano and D. Dill, Phys. Rev. A **6**, 185 (1972); U. Fano, J. Opt. Soc. Am. **65**, 979 (1975); Phys. Rev. A **32**, 617 (1985).
[14] K. T. Lu and U. Fano, Phys. Rev. A **2**, 81 (1970); D. Dill and U. Fano, Phys. Rev. Lett. **29**, 1203 (1972); A. Guistisuzor and U. Fano, J. Phys. B **17**, 215 (1984).
[15] C. M. Lee and K. T. Lu, Phys Rev. A **8**, 1241 (1973); D. Dill, *ibid.* **7**, 1976 (1973).
[16] C. H. Greene and CH. Jungen. Adv. At. Mol. Phys. **21**, 51 (1985).
[17] C. H. Greene and L. Kim, Phys. Rev. A **36**, 2706 (1987).
[18] P. F. O'Mahony and C. H. Greene, Phys. Rev. A **31**, 250 (1985); L. Kim and C. H. Greene, *ibid.* **36**, 4272 (1987).
[19] D. J. Armstrong, R. P. Wood, and C. H. Greene, Phys. Rev. A **47**, 1981 (1933); R. P. Wood and C. H. Greene, *ibid.* **49**, 1029 (1994).
[20] Ch. Jungen and D. Dill, J. Chem. Phys. **73**, 3338 (1980); H. Gao, Ch. Jungen, and C. H. Greene, Phys. Rev. A **47**, 4877 (1993).
[21] Y. L. Shao, C. Fotakis, and D. Charalambidis, Phys. Rev. A **48**, 3636 (1993).
[22] T. N. Chang and X. Tang. Phys. Rev. **46**, 2209 (1992).
[23] R. Moccia and P. Spizzo, J. Phys. B **21**, 1121 (1988).
[24] G. W. Schinn, C. J. Dai, and T. F. Gallagher (unpublished). (Note that the data here combined with those presented in Ref. [6] are from the same experiment, which mainly concerns the profiles of the Mg $3pns$ states.)